

# Nanoscale

Accepted Manuscript



This is an *Accepted Manuscript*, which has been through the Royal Society of Chemistry peer review process and has been accepted for publication.

*Accepted Manuscripts* are published online shortly after acceptance, before technical editing, formatting and proof reading. Using this free service, authors can make their results available to the community, in citable form, before we publish the edited article. We will replace this *Accepted Manuscript* with the edited and formatted *Advance Article* as soon as it is available.

You can find more information about *Accepted Manuscripts* in the [Information for Authors](#).

Please note that technical editing may introduce minor changes to the text and/or graphics, which may alter content. The journal's standard [Terms & Conditions](#) and the [Ethical guidelines](#) still apply. In no event shall the Royal Society of Chemistry be held responsible for any errors or omissions in this *Accepted Manuscript* or any consequences arising from the use of any information it contains.

## COMMUNICATION

## High-performance $n$ -MoS<sub>2</sub>/ $i$ -SiO<sub>2</sub>/ $p$ -Si heterojunction solar cells

Cite this: DOI: 10.1039/x0xx00000x

L. Z. Hao,<sup>a\*</sup> W. Gao,<sup>a</sup> Y. J. Liu,<sup>a</sup> Z. D. Han,<sup>a</sup> Q. Z. Xue,<sup>a</sup> W. Y. Guo,<sup>a</sup> J. Zhu<sup>b</sup> and Y. R. Li<sup>b\*</sup>

Received 00th January 2015,

Accepted 00th January 2015

DOI: 10.1039/x0xx00000x

www.rsc.org/

**A solar cell based on  $n$ -MoS<sub>2</sub>/ $i$ -SiO<sub>2</sub>/ $p$ -Si heterojunction is fabricated. The device exhibits a high power-conversion efficiency of 4.5% due to the incorporation of a nano-scale SiO<sub>2</sub> buffer into the MoS<sub>2</sub>/Si interface. The present device architectures are envisaged as potentially valuable candidates for high-performance photovoltaic devices.**

In recent years, two dimensional layered materials, such as molybdenum disulfide (MoS<sub>2</sub>) and graphene, have manifested a lot of intriguing properties and spurred intense scientific interests.<sup>1,2</sup> Due to the strong absorption to sunlight, MoS<sub>2</sub> has attracted much interest in developing high-performance solar cells. It has been reported that MoS<sub>2</sub> exhibits one order of magnitude higher sunlight absorption than the most commonly used solar absorbers of Si and GaAs.<sup>3</sup> Intrinsic MoS<sub>2</sub> belongs  $n$ -type semiconductors and its band gap is 1.2-1.9 eV.<sup>4</sup> Based on the configuration of Schottky or  $p$ - $n$  junctions, several kinds of MoS<sub>2</sub>-based high-speed photodetectors and new-type solar cells were constructed.<sup>5-8</sup> Shanmugan et al. achieved a power conversion efficiency (PCE) of 1.8% in Au/MoS<sub>2</sub> junctions.<sup>6</sup> Further, Wi et al. utilized the plasma-induced  $p$ -doping approach to form  $p$ - $n$  junctions in MoS<sub>2</sub> layers.<sup>7</sup> The devices showed good photovoltaic properties with a large short-circuit photocurrent density of 20.9 mAcm<sup>-2</sup> and a high PCE of 2.8%. Presently, Si is dominating the commercial photovoltaic market due to its high abundance and mature processing technology. In order to develop practically applicable solar cells, it is of great valuable to realize the integration of MoS<sub>2</sub> on Si. By stacking a MoS<sub>2</sub> monolayer on Si to enhance light absorption, Tsai et al. realized the increase of the PCE from 4.64% to 5.23% in Al/Si solar cells.<sup>8</sup> It can be expected that the MoS<sub>2</sub>/Si heterojunctions would become one of good candidates to develop high-performance solar cells. MoS<sub>2</sub> has a layered crystal structure, where the atoms in layers are hexagonally packed, while crystal Si belongs to diamond-like structure. The large difference of the lattice structure between them would result in large quantities of lattice defects at the interface when MoS<sub>2</sub> films were deposited straight on Si surface.<sup>9</sup> Additionally, inherent reactivity and serious element diffusion at the interface are unavoidable during the integration. These interfacial characteristics can degrade largely the performance of the solar cells. Thus, it is necessary to conduct interface modification before making viable functional devices on

Si. Previous studies show that employing suitable buffers at the interface, such as ZnO,<sup>10</sup> Al<sub>2</sub>O<sub>3</sub>,<sup>11</sup> and MoO<sub>3</sub>,<sup>12</sup> is one of effective ways to implement interface modification in junction-type solar cells. The buffer can balance carrier injection and reduce leakage current. Especially in the case of band edge modifications, a large open circuit voltage can be achieved through built-in barrier enhancement when the buffers with a large band gap are incorporated.<sup>13</sup> Apart from the MoS<sub>2</sub> and Si themselves, a suitable buffer would be important to obtain high-performance MoS<sub>2</sub>/Si solar cells. However, the related studies are absent.

In this work, MoS<sub>2</sub> bulk-like thin films were deposited on SiO<sub>2</sub> buffered  $p$ -type Si substrates and MoS<sub>2</sub>/SiO<sub>2</sub>/Si  $n$ - $i$ - $p$  junction solar cells were fabricated. SiO<sub>2</sub> was chosen as a buffer for three reasons. Firstly, formation of SiO<sub>2</sub> layers at high temperatures in oxidizing atmosphere can form an SiO<sub>2</sub>/Si interface with low interface state density ( $<1 \times 10^{10}/\text{cm}^2\text{eV}$ ).<sup>14</sup> Secondly, SiO<sub>2</sub>/Si is usually used as the substrate to obtain large-scale uniform MoS<sub>2</sub> monolayers.<sup>15</sup> Finally, SiO<sub>2</sub> as an insulating buffer can decrease the carrier recombination near the interface and improve the photovoltaic properties of the devices.<sup>16</sup> Our results demonstrated that the performance of the device was enhanced significantly due to the insertion of the nano-scale SiO<sub>2</sub> buffer into the MoS<sub>2</sub>/Si interface. According to the results, the mechanisms of the enhanced photovoltaic properties were discussed in terms of the energy-band structure near the interface.

MoS<sub>2</sub> bulk-like thin films were deposited on (100)-oriented Si substrates using dc magnetron sputtering technique. The precursor materials for the films were MoS<sub>2</sub> powders. The MoS<sub>2</sub> powders (purity, 99.9%) were cold-pressed into a disk under the pressure of 20.0 MPa. The as-fabricated disk ( $\Phi 60.0$  mm $\times$ 4.5 mm) was used as the target during sputtering. The Si substrates (size, 10 mm $\times$ 10 mm) used in this work are  $p$ -type semiconductors with the resistivity of 1.2-1.8  $\Omega$  cm. Before the deposition, the substrates were ultrasonically cleaned in sequence by alcohol, acetone, and de-ionized water. Then, the substrates were dipped into HF solution ( $\sim 5.0\%$ ) for 60s to remove the natural oxide layer from the Si surface. After that, the substrates were annealed at 600  $^{\circ}\text{C}$  under the oxygen pressure of 20 Pa for 3 min to form SiO<sub>2</sub> buffer layer on the Si surface. The thickness of the SiO<sub>2</sub> layer is about 3-5 nm calculated from the capacitance-voltage ( $C$ - $V$ ) curve of the SiO<sub>2</sub>/Si heterojunction. Subsequently,  $\sim 40$ -nm-thickness MoS<sub>2</sub> thin films

were deposited. During the deposition, the working pressure of argon gas and deposition temperature were 0.3 Pa and 380.0 °C, respectively. Finally, the top ~30-nm-thickness Pd electrode was fabricated on the MoS<sub>2</sub> film using dc magnetron sputtering technique. The whole top surface of the film was covered by the electrode layer. The back ~200-nm-thickness indium (In) electrode was fabricated on the whole backside of the Si substrate using thermal evaporation. The thickness of the MoS<sub>2</sub> films and electrode layers were calibrated by scanning electron microscope (SEM). Comparatively, MoS<sub>2</sub> films were also deposited straight on the Si surface to form *n-p* junctions as reference devices.

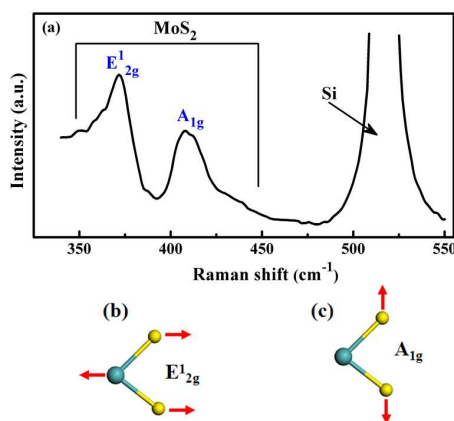


Fig. 1 (a) Raman spectrum of the MoS<sub>2</sub> films on SiO<sub>2</sub> buffered Si substrates. (b) and (c) Schematic illustrations of the oscillating mode of E<sub>12g</sub> and A<sub>1g</sub>, respectively. Atom color code: light blue-green, Mo; yellow, S.

Fig. 1a shows the Raman spectrum of the MoS<sub>2</sub> film on SiO<sub>2</sub>/Si. From the figure, we can see that the film exhibits two characteristic MoS<sub>2</sub> Raman peaks, the E<sub>12g</sub> mode at ~373 cm<sup>-1</sup> and A<sub>1g</sub> mode at ~407 cm<sup>-1</sup>. The E<sub>12g</sub> mode corresponds to the sulfur and molybdenum atoms oscillating in antiphase parallel to the crystal plane, as shown in Fig. 1b, and the A<sub>1g</sub> mode corresponds to the sulfur atoms oscillating in antiphase out-of-plane, as shown in Fig. 1c. Our Raman results are consistent with other reported results about MoS<sub>2</sub> bulk-like films.<sup>17</sup> The separation between Raman peaks

of the film,  $\Delta=34$  cm<sup>-1</sup>, is much larger than those for the reported monolayer and several-layer MoS<sub>2</sub>.<sup>18</sup> As shown in the figure, the peak intensity of E<sub>12g</sub> is higher than the A<sub>1g</sub> peak. This is similar to the results from previous reports,<sup>9,19</sup> and indicative of high structural quality in the as-deposited MoS<sub>2</sub> film.

Fig. 2a shows the schematic illustration of the electrical measurement of the Pd/MoS<sub>2</sub>/SiO<sub>2</sub>/Si/In solar cell. Forward voltages are defined as positive voltages applied on In electrode. Pure MoS<sub>2</sub> belongs to *n*-type semiconductors.<sup>4,6,17</sup> Thus, the *n-p* and *n-i-p* junctions were formed when the films were deposited on *p*-Si and SiO<sub>2</sub> buffered Si, respectively. Fig. 2b shows the dark current density versus voltage (*J-V*) curves of the devices with/without a SiO<sub>2</sub> buffer. Both the devices exhibit obvious rectifying behaviour. In our experiments, the contacts of Pd/MoS<sub>2</sub> and In/Si are almost ohmic. Thus, the asymmetric characteristics of the *J-V* curves originate mainly from MoS<sub>2</sub>/Si and MoS<sub>2</sub>/SiO<sub>2</sub>/Si contacts, respectively. The turn-on voltage (*V*<sub>on</sub>) of 0.19 V for the MoS<sub>2</sub>/Si *n-p* junction, at which the current starts to increase rapidly,<sup>20</sup> can be obtained. From the figure, we can see that the *V*<sub>on</sub> increases to 0.33 V for the MoS<sub>2</sub>/SiO<sub>2</sub>/Si *n-i-p* junction. Fig. 2c shows the replot of the *J-V* curves in the forward voltage range using semi-logarithmic mode. For the *n-p* junction, three distinctly different linear regions with different ideality factor (*n*) can be observed. This demonstrates that the conduction of the *n-p* junction is dominated by diffusion current (*n*=1.0), recombination current (*n*=2.0), and trap-assisted recombination current (*n*=9.0) in different forward voltage range, respectively. This is similar with the reported results about other *p-n* junctions.<sup>21</sup> When the SiO<sub>2</sub> buffer is incorporated, the currents are suppressed largely and the transporting mechanisms are changed in high voltage range, as shown in the figure. Fig. 2d shows the replot of the dark *J-V* curve of the *n-i-p* junction using Fowler-Nordheim (F-N) tunnelling mechanism. The tunnelling current density is described as<sup>22</sup>

$$J = AV^2 \exp(-B/V), \quad (1)$$

where *A* and *B* are constants. As shown in the figure, the dependence of Log(*JV*<sup>-2</sup>) on *V*<sup>-1</sup> is almost linear when the voltage is larger than *V*<sub>on</sub> (0.33V). This implies that the carriers in the *n-i-p* junction can pass the SiO<sub>2</sub> layer by F-N tunnelling.

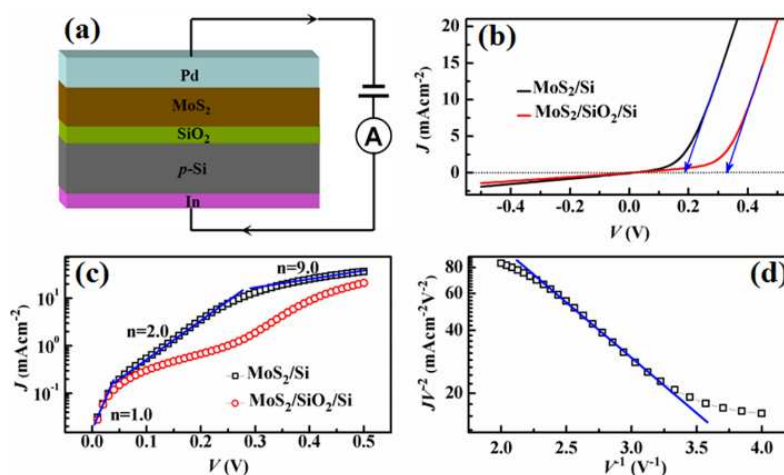


Fig. 2 (a) Schematic illustration of the electrical measurement of the Pd/MoS<sub>2</sub>/SiO<sub>2</sub>/Si/In solar cell. (b) Dark *J-V* curves of the fabricated devices with/without SiO<sub>2</sub> buffer layer. (c) Replots of the dark *J-V* curves in the forward voltage range using semi-logarithmic mode. (d) Replot of the dark *J-V* curve of the Pd/MoS<sub>2</sub>/SiO<sub>2</sub>/Si/In solar cell in the forward voltage range using F-N tunnelling mechanism.

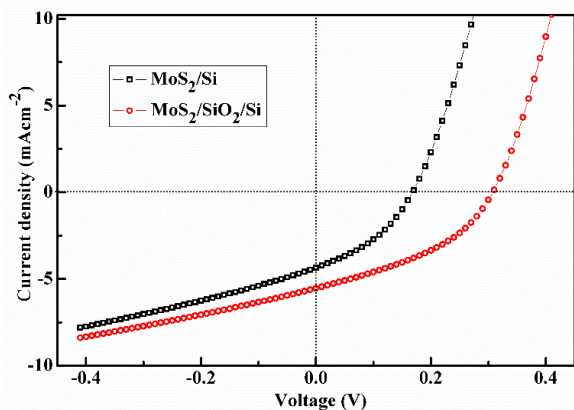


Fig. 3 Photovoltaic characteristics of the solar cell devices with/without SiO<sub>2</sub> buffer layer under 15mWcm<sup>-2</sup> light illumination.

Fig. 3 shows the photovoltaic characteristics of the devices without and with a SiO<sub>2</sub> buffer under 15.0 mWcm<sup>-2</sup> light illuminations. The MoS<sub>2</sub>/Si *n-p* junction shows an open-circuit voltage ( $V_{OC}$ ) of 0.15 V and a short-circuit current ( $J_{SC}$ ) of 4.3 mAcm<sup>-2</sup>. It has a fill factor ( $FF$ ) of 0.39, resulting in a PCE of merely 1.4%. When the SiO<sub>2</sub> buffer is introduced, the photovoltaic performance is enhanced significantly, as shown in the figure. For the Pd/MoS<sub>2</sub>/SiO<sub>2</sub>/Si/In cell,  $V_{OC}$  increases to 0.3 V, an enhancement of 2 times. Simultaneously,  $J_{SC}$  and  $FF$  of the device increases to 5.5 mAcm<sup>-2</sup> and 0.42, respectively. The overall PCE reaches 4.5%, up to a 3-fold increase compared to the reference device. This PCE is the highest value among all the reported MoS<sub>2</sub>-based solar cells.<sup>4-6</sup> Thus, the insertion of the SiO<sub>2</sub> buffer at the MoS<sub>2</sub>/Si interface plays a crucial role on improving the light-to-current conversion efficiency for the solar cells.

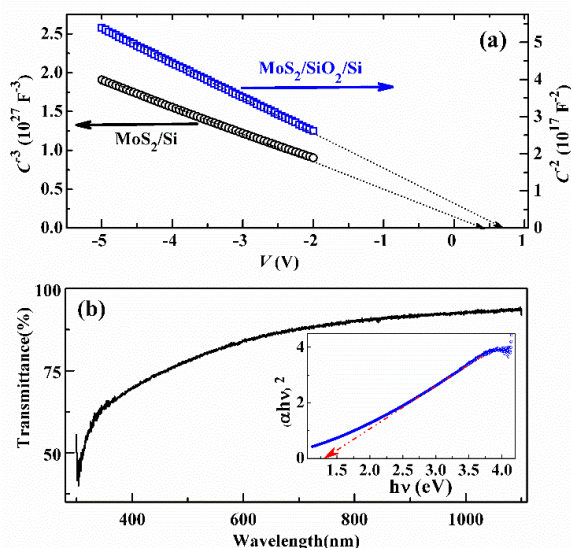


Fig. 4 (a)  $C^{-3}$  versus  $V$  curve of the MoS<sub>2</sub>/Si *n-p* junction and  $C^{-2}$  versus  $V$  curve of the MoS<sub>2</sub>/SiO<sub>2</sub>/Si *n-i-p* junction measured at 1MHz frequency, respectively. (b) Transmission spectrum of the MoS<sub>2</sub> film deposited on glass substrate under the same growth condition with the film on Si. The inset shows a plot of  $(ahv)^2$  versus  $h\nu$ .

According to the measured  $C-V$  curve in the reverse voltage range,  $C^{-3}$  versus voltage curve for the *n-p* junction and  $C^{-2}$  versus voltage curve for the *n-i-p* junction are shown in Fig. 4a. In a semiconductor junction, the capacitance can be expressed as<sup>23</sup>

$$C \propto (V+V_{bi})^{-1/m}, \quad (2)$$

where  $C$  is the capacitance,  $V$  is the reverse voltage, and  $V_{bi}$  is the built-in electrical field.  $m$  is a constant,  $m=2$  for an abrupt junction and  $m=3$  for a graded junction.<sup>24</sup> The linear dependence demonstrates that the MoS<sub>2</sub>/Si *n-p* junction is graded, while the MoS<sub>2</sub>/SiO<sub>2</sub>/Si *n-i-p* junction is abrupt. According to the intercept on voltage axis,  $V_{bi}$  can be determined. As shown in the figure, the  $V_{bi}$  is enhanced due to the introduction of the SiO<sub>2</sub> buffer. According to the extracted results, the  $V_{bi}$  of the *n-i-p* junction is about 0.65 V, which is larger than 0.41 V of the *n-p* junction. Fig. 4b shows the transmission spectrum of the ~40-nm-thickness MoS<sub>2</sub> film deposited on glass (a-SiO<sub>2</sub>) substrate under the same growth condition with that on Si. From the figure, we can see that the film has high transmittance (>50%) in the visible light range. It can be deduced that only a part of incident lights is absorbed by the MoS<sub>2</sub> film when the junction is under the light illumination and others can reach the Si substrate. Thus, photo-induced carriers can be generated in both the film and Si substrate. As shown in the inset,  $(ahv)^2$  is plotted as a function of photon energy  $h\nu$ , wherein  $h$  is the Planck constant and  $\nu$  is photon frequency. The  $\alpha$  is the absorption coefficient, calculated by  $\alpha d = \ln(1/T)$ ,  $d$  and  $T$  are thickness and transmittance of the film, respectively.<sup>25</sup> The band gap ( $E_g$ ) of the film can be determined by the intercept of the line on  $h\nu$  axis,  $E_g=1.42$  eV. The energy-band value for the film is a little larger than MoS<sub>2</sub> bulk (~1.2 eV) and much smaller than the monolayer (~1.9 eV).

The observed enhanced photovoltaic characteristics can be explained by considering the modulation of the SiO<sub>2</sub> buffer on the energy-band alignment near the MoS<sub>2</sub>/Si interface. Fig. 5a shows the energy band diagram of MoS<sub>2</sub>/Si *n-p* junction. By the Hall Effect measurements, the MoS<sub>2</sub> film is proved to be a quasi-intrinsic semiconductor with a very small Hall coefficient (~0). Due to the quasi-intrinsic semiconductor nature, the Fermi energy level of the MoS<sub>2</sub> film ( $E_{F1}$ ) is close to (but above) the middle of the energy band gap. As shown in Fig. 4b, the energy-band gap of the MoS<sub>2</sub> film ( $E_{g1}$ ) is 1.42 eV. For single-crystal *p*-Si, the Fermi energy level [ $E_{F2}=5.0$  eV] and energy band gap [ $E_{g2}=1.12$  eV] are taken to construct the band structure and the difference ( $E_{F2}-E_{V2}$ ) between the Fermi energy level and the top of the valence band is about 0.2 eV.<sup>26</sup> When the MoS<sub>2</sub> film is deposited straight on the surface of *p*-type Si, a MoS<sub>2</sub>/Si *n-p* junction is fabricated and the built-in field is formed near the MoS<sub>2</sub>/Si interface. The built-in field points from the film to substrate and it can be expressed as  $V_{bi}=(E_{F2}-E_{F1})/e$ .<sup>27</sup> According to the  $V_{bi}$  of 0.41 V obtained from Fig. 4a, the Fermi energy level of the MoS<sub>2</sub> film ( $E_{F1}$ ) can be determined, about 4.59 eV. This value is in accord with the reported results.<sup>28</sup> Under light illumination, the incident photons can be absorbed by both the MoS<sub>2</sub> film and Si, as demonstrated in Fig. 4b, and the electron-hole (*e-h*) pairs are generated in both the sides of the junction. The built-in field facilitates the separation of photo-generated *e-h* pairs, transporting separated electrons from Si to MoS<sub>2</sub> and holes towards Si. The processes of photo-excitation and carrier transport in the junction are illustrated in Fig. 5a. Therefore, photovoltaic characteristics are exhibited. In junction-type solar cells, the  $V_{OC}$  is closely related to the built-in field.<sup>29</sup> The relative small value of the  $V_{bi}$  in the *n-p* junction results in a small  $V_{OC}$  of only 0.15 V and a low PCE of 1.4%. When the buffer is inserted into the MoS<sub>2</sub>/Si interface, the

SiO<sub>2</sub> layer instead of the Si surface forms a contact with the MoS<sub>2</sub> film. As an insulator, SiO<sub>2</sub> has a larger work function of about 5.4 eV than Si.<sup>30</sup> The larger work function led to a larger  $V_{bi}$  of 0.65 V, as shown in Fig. 4a. The increase of  $V_{bi}$  further enhanced the separation of photo-generated  $e-h$  pairs in the junction and a larger  $V_{OC}$  of 0.3 V was obtained. Additionally, the photo-generated carriers in the  $n-i-p$  junction can pass the SiO<sub>2</sub> layer with the F-N tunnelling mechanism because the  $V_{bi}$  of 0.65 V is larger than the  $V_{on}$ , as shown in Fig. 5b. This results in a large  $J_{SC}$  of 5.5 mAcm<sup>-2</sup>. Both the large  $V_{OC}$  and  $J_{SC}$  promise a high PCE of 4.5% in the  $n-i-p$  junction. Based on the above analysis, definitely, the SiO<sub>2</sub> buffer plays a crucial role to obtain the enhanced performance. A certain thickness of the SiO<sub>2</sub> layer was necessary to have good passivation of the Si surface. The optimized SiO<sub>2</sub> thickness is several nanometers according to other reported results.<sup>31</sup> This is in accord with our studies. However, if the SiO<sub>2</sub> layer is too thick, it can decrease the effectiveness of the carrier tunnelling due to the scattering and trapping of the carriers in the SiO<sub>2</sub> layer.<sup>32</sup> At the same time, the SiO<sub>2</sub> layer offers a high potential barrier prevent the carriers from the diffusion and shift moving to two ends. Thus, the electrical performance of the fabricated solar cells would be degraded. In our experiments, the photovoltaic characteristics disappeared completely when the thickness of the SiO<sub>2</sub> layer was larger than ~10.0 nm.

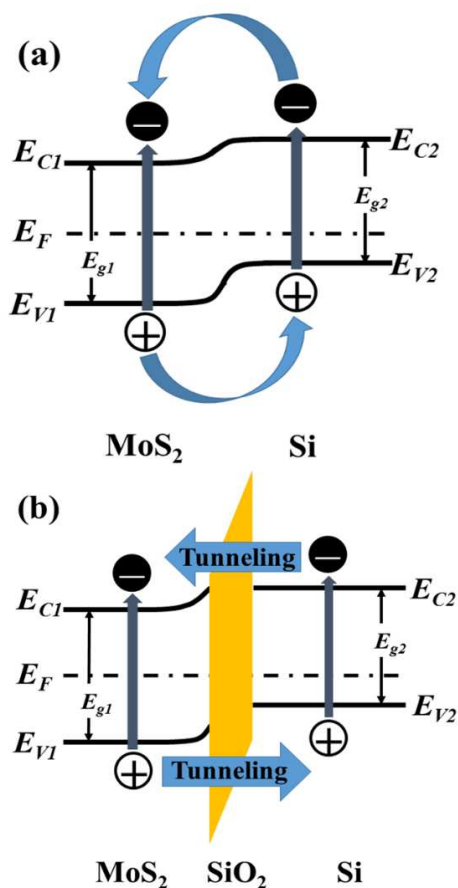


Fig. 5 (a) Energy band diagram of MoS<sub>2</sub>/Si  $n-p$  junction. (b) Energy band diagram of MoS<sub>2</sub>/SiO<sub>2</sub>/Si  $n-i-p$  junction.  $E_g$  is energy band gap,  $E_F$  is Fermi-energy level,  $E_C$  is the bottom of conduction band, and  $E_V$  is the top of valence band.

In summary, MoS<sub>2</sub> bulk-like thin films were deposited on SiO<sub>2</sub> buffered  $p$ -type Si substrates and MoS<sub>2</sub>/SiO<sub>2</sub>/Si  $n-i-p$  junctions were formed. Our results demonstrated that the photovoltaic performance of the device was enhanced significantly due to the incorporation of

the SiO<sub>2</sub> buffer. The  $V_{OC}$  and  $J_{SC}$  increased to 0.3 V and 5.5 mAcm<sup>-2</sup>, respectively. The PCE of 4.5% was achieved, which was the highest value among all the reported MoS<sub>2</sub>-based solar cells. Besides the expected improvement of the interfacial structures by the passivation, the SiO<sub>2</sub> buffer can effectively enhance the built-in field and further promote the separation of photo-generated  $e-h$  pairs in the junction. All these should be responsible for the enhanced photovoltaic performance. Our work supplies an effective route for the integration of MoS<sub>2</sub> films with Si-based electronics to develop high-performance solar cells.

## Acknowledgements

The authors would like to acknowledge the financial support by the Fundamental Research Funds for the Central Universities (14CX05038A) and the National Science Foundation of China (Grant Nos. 51102284 and 51372030).

## Notes and references

<sup>a</sup>College of Science, China University of Petroleum, Qingdao, Shandong 266580, People's Republic of China. *E-mail*: haolanzhong@upc.edu.cn

<sup>b</sup>State Key Laboratory of Electronic Thin Films and Integrated Devices, University of Electronic Science and Technology of China, Chengdu 610054, People's Republic of China. *E-mail*: yrli@upc.edu.cn

- 1 S. Behura and V. Berry, *ACS Nano*, 2015, **9**, 2227; Q. Ji, Y. Zhang, T. Gao, Y. Zhang, D. Ma, M. Liu, Y. Chen, X. Qiao, P. Tan, M. Kan, J. Feng, Q. Sun and Z. Liu, *Nano Lett.*, 2013, **13**, 3870;
- 2 W. Jie, F. Zheng and J. Hao, *Appl. Phys. Lett.*, 2013, **103**, 233111; W. Jie and J. Hao, *Nano Scale*, 2014, **6**, 6346; T. Zhang, Q. Xue, S. Zhang and M. Dong, *Nano Today*, 2012, **7**, 180.
- 3 M. Bernardi, M. Palummo and J. C. Grossman, *Nano Lett.*, 2013, **13**, 3664.
- 4 K. F. Mak, C. Lee, J. Hone, J. Shan and T. F. Heinz, *Phys. Rev. Lett.*, 2010, **105**, 136805.
- 5 M. R. Esmaili-Rad and S. Salahuddin, *Sci. Rep.*, 2013, **3**, 2345; M. M. Furchi, A. Pospischil, F. Libisch, J. Burgdörfer and T. Mueller, *Nano Lett.*, 2014, **14**, 4785; R. Cheng, D. Li, H. Zhou, C. Wang, A. Yin, S. Jiang, Y. Liu, Y. Chen, Y. Huang and X. Duan, *Nano Lett.*, 2014, **14**, 5590; S. Sutar, P. Agnihotri, E. Comfort, T. Taniguchi, K. Watanabe and J. U. Lee, *Appl. Phys. Lett.*, 2014, **104**, 122104.
- 6 M. Shanmugam, C. A. Durcan and B. Yu, *Nanoscale*, 2012, **4**, 7399.
- 7 S. Wi, H. Kim, M. Chen, H. Nam, L. J. Guo, E. Meyhofer and X. Liang, *ACS Nano*, 2014, **8**, 5270.
- 8 M. L. Tsai, S. H. Su, J. K. Chang, D. S. Tsai, C. H. Chen, C. I. Wu, L. J. Li, L. J. Chen and J. H. He, *ACS Nano*, 2014, **8**, 8317.
- 9 M. R. Laskar, L. Ma, S. Kannappan, P. S. Park, S. Krishnamoorthy, D. N. Nath, W. Lu, Y. Wu and S. Rajan, *Appl. Phys. Lett.*, 2013, **102**, 252108.
- 10 Z. Fan, K. Yao and John Wang, *Appl. Phys. Lett.*, 2014, **105**, 162903.
- 11 X. Y. Tan, X. Z. Zhang, C. H. Wang, X. L. Gao, H. Lin and J. Zhang, *Jpn. J. Appl. Phys.*, 2011, **50**, 070204.
- 12 L. Cattin, F. Dahou, Y. Lare, M. Morsli, R. Tricot, S. Houari, A. Mokrani, K. Jondo, A. Khelil, K. Napo and J. C. Bernède, *J. Appl. Phys.*, 2009, **105**, 034507.
- 13 W. Wu, Y. Cao, J. V. Caspar, Q. Guo, L. K. Johnson, R. S. Mclean, I. Malajovich and K. R. Choudhury, *Appl. Phys. Lett.*, 2014, **105**, 042108.

- 14 G. Declerck, R. Van Overstraeten and G. Broux, *Solid-State Electron*, 1973, **16**, 1451; T. Matsumoto, R. Hirose, F. Shibata, D. Ishibashi, S. Ogawara and H. Kobayashi, *Sol. Energy Mater. Sol. Cells*, 2015, **134**, 298.
- 15 D. J. Late, B. Liu, H. S. S. Ramakrishna Matte, C. N. R. Rao and V. P. Dravid, *Adv. Funct. Mater.*, 2012, **22**, 1894; D. J. Late, B. Liu, H. S. S. Ramakrishna Matte, V. P. Dravid and C. N. R. Rao, *ACS Nano*, 2012, **6**, 5635.
- 16 G. Bugnon, G. Parascandolo, S. Hänni, M. Stuckelberger, M. Charrière, M. Despeisse, F. Meillaud and C. Ballif, *Sol. Energy Mater. Sol. Cells*, 2014, **120**, 143.
- 17 D. J. Late, P. A. Shaikh, R. Khare, R. V. Kashid, M. Chaudhary, M. A. More and S. B. Ogale, *ACS Appl. Mater. Interfaces*, 2014, **6**, 15881.
- 18 R. Ganatra and Q. Zhang, *ACS Nano*, 2014, **8**, 4074; Y. H. Lee, X. Q. Zhang, W. Zhang, M. T. Chang, C. T. Lin, K. D. Chang, Y. C. Yu, J. T. W. Wang, C. S. Chang, L. J. Li, and T. W. Lin, *Adv. Mater.*, 2012, **24**, 2320.
- 19 Y. Zhan, Z. Liu, S. Najmaei, P. M. Ajayan and J. Lou, *Small*, 2012, **8**, 966.
- 20 H. Yang, H. M. Luo, H. Wang, I. O. Usov, N. A. Suvorova, M. Jain, D. M. Feldmann, P. C. Dowden, R. F. DePaula and Q. X. Jia, *Appl. Phys. Lett.*, 2008, **92**, 102113.
- 21 W. Du, M. Baba, K. Toko, K. O. Hara, K. Watanabe, T. Sekiguchi, N. Usami and T. Suemasu, *J. Appl. Phys.*, 2014, **115**, 223701.
- 22 L. Hao, Q. Xue, X. Gao, Q. Li, Q. Zheng, and K. Yan, *Appl. Phys. Lett.*, 2007, **91**, 212105.
- 23 E. W. Lee II, L. Ma, D. N. Nath, C. H. Lee, A. Arehart, Y. Wu and S. Rajan, *Appl. Phys. Lett.*, 2014, **105**, 203504.
- 24 H. Huang, G. Fang, X. Mo, L. Yuan, H. Zhou, M. Wang, H. Xiao and X. Zhao, *Appl. Phys. Lett.*, 2009, **94**, 063512.
- 25 X. Chen, K. Ruan, G. Wu and D. Bao, *Appl. Phys. Lett.*, 2008, **93**, 112112.
- 26 S. M. Sze and K. K. Ng, *Physics of Semiconductor Devices*, Wiley, New York, 3rd edn, 2007.
- 27 Donald A. Neamen, *Semiconductor Physics and Devices: Basic Principles*, McGraw-Hill, New York, 2003.
- 28 M. Fontana, T. Deppe, A. K. Boyd, M. Rinzan, A. Y. Liu, M. Paranjape and P. Barbara, *Sci. Rep.*, 2013, **3**, 1634.
- 29 J. Shewchun, J. Dubow, A. Myszkowski and R. Singh, *J. Appl. Phys.*, 1978, **49**, 855.
- 30 J. Robertson and B. Falabretti, *J. Appl. Phys.*, 2006, **100**, 014111.
- 31 H. W. Du, J. Yang, Y. H. Li, F. Xu, J. Xu, and Z. Q. Ma, *Appl. Phys. Lett.*, 2015, **106**, 093508; H. W. Fang, S. J. Liu, T. E. Hsieh, J. Y. Juang and J. H. Hsieh, *Sol. Energy Mater. Sol. Cells*, 2011, **85**, 2589; V. Vasu and A. Subrahmanyam, *Semicond. Sci. Technol.*, 1992, **7**, 320.
- 32 J. Sheng, K. Fan, D. Wang, C. Han, J. Fang, P. Gao and J. Ye, *ACS Appl. Mater. Interfaces*, 2014, **6**, 16027.